Quantifying Intrinsic, Extrinsic, Dielectric, and Secondary Pyroelectric Responses in $PbZr_{1-x}Ti_xO_3$ Thin Films

Gabriel Velarde,[†] Shishir Pandya,[†] Lei Zhang,[†] David Garcia,[†] Eduardo Lupi,[†] Ran Gao,[†] Joshua D. Wilbur,[‡] Chris Dames,[‡] and Lane W. Martin*[,†,§]

[†]Department of Materials Science and Engineering, University of California, Berkeley, Berkeley, California 94720, United States
[‡]Department of Mechanical Engineering, University of California, Berkeley, Berkeley, California 94720, United States
[§]Materials Sciences Division, Lawrence Berkeley National Laboratory, Berkeley, California 94720, United States

ABSTRACT: Applications such as solid-state waste-heat energy conversion, infrared sensing, and thermally-driven electron emission rely on pyroelectric materials (a subclass of dielectric piezoelectrics) which exhibit temperature-dependent changes in polarization. Although enhanced dielectric and piezoelectric responses are typically found at polarization instabilities such as temperature- and chemically induced phase boundaries, large pyroelectric effects have been primarily limited in study to temperature-induced phase boundaries. Here, we directly identify the magnitude and sign of the intrinsic, extrinsic, dielectric, and secondary pyroelectric contributions to the total pyroelectric response as a function of chemistry in thin films of the canonical ferroelectric $PbZr_{1-x}Ti_xO_3$ (x = 0.40, 0.48, 0.60, and 0.80) across the morphotropic phase boundary. Using phase-sensitive frequency and applied dc-bias methods, the various pyroelectric contributions were measured. It is found that the total pyroelectric response decreases systematically as one moves from higher to lower titanium contents. This arises from a combination of decreasing intrinsic response (−232 to −97 μC m^{-2} K^{-1}) and a sign inversion (+33 to −17 μC m^{-2} K^{-1}) of the extrinsic contribution upon crossing the morphotropic phase boundary. Additionally, the measured secondary and dielectric contributions span between −70 and −29 and 10−115 μC m^{-2} K^{-1} under applied fields, respectively, following closely trends in the piezoelectric and dielectric susceptibility. These findings and methodologies provide novel insights into the understudied realm of pyroelectric response.

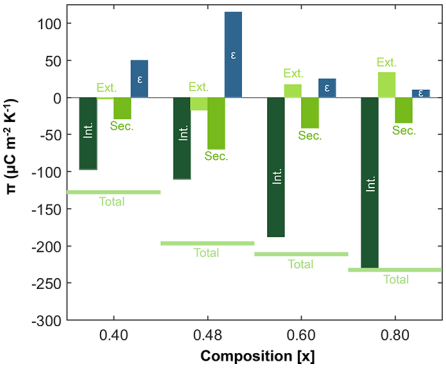

INTRODUCTION

Among the various interrelationships of electrical, mechanical, and thermal properties of polar materials, electrothermal effects have remained relatively understudied as a result of limited materials physics understanding, insufficient access to well-controlled materials, and inadequate measurement protocols.[1] One particularly important effect in this regard is the pyroelectric effect which is parametrized by the pyroelectric coefficient

$$\pi = \left(\frac{\partial P_s}{\partial T}\right)_{E,X} \quad (1)$$

where X, P_s, T, and E refer to stress, spontaneous polarization, temperature, and electric field, respectively.[2] While considerable advances in controlling both dielectric (E) and piezoelectric (X) responses have been made, there are limited developments over the past few decades in the understanding of routes to enhance π. While there are a number of commercial applications for pyroelectrics (e.g., infrared sensors for thermal imaging, pollutant detection, etc.[3,4]), these typically rely on materials such as $LiTaO_3$, $LiNbO_3$, and triglycine sulfate which have rather unremarkable room-temperature π values, but other features (e.g., low dielectric permittivity) that make them useful for some applications. In turn, the development of new materials with large π or routes to enhance π in existing materials has led to reports of enhanced electrothermal responses, generally accomplished by placing the material in proximity to a temperature-induced phase boundary.[5] While this provides for impressive values of π, the effects are enhanced only in a narrow temperature regime (e.g., near the ferroelectric-to-paraelectric phase boundary occurring at the Curie temperature, T_C). Nonetheless, there is considerably less work on the same phenomena in proximity to chemically induced phase boundaries. While it is well-known that both dielectric and piezoelectric response can be enhanced in the vicinity of features like the morphotropic phase boundary (MPB),[6−9] few, and often conflicting, reports

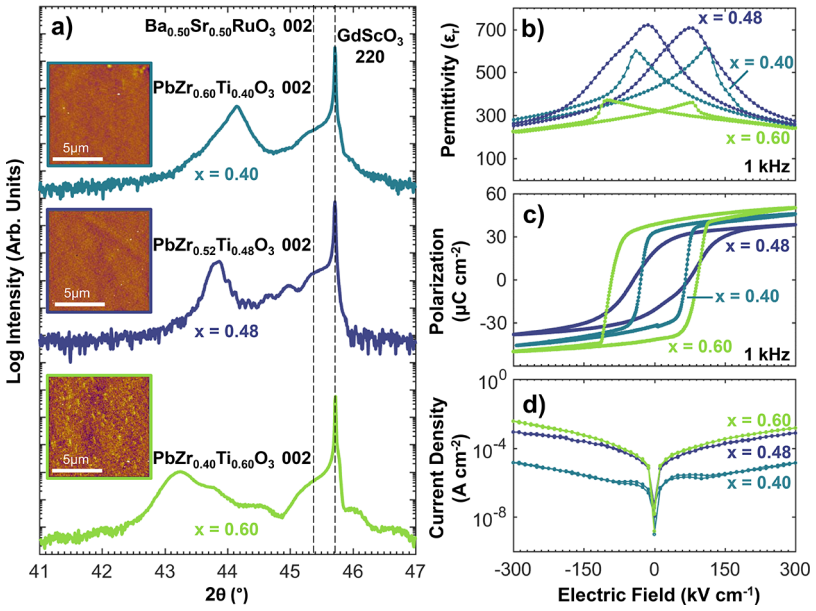

Figure 1. Structural and (di)electrical measurements of $PbZr_{1-x}Ti_xO_3$ heterostructures. (a) X-ray diffraction line scans of x = 0.40, 0.48, and 0.60 heterostructures (bottom to top) about the $GdScO_3$ 220-diffraction condition. Insets display the respective atomic force microscopy surface morphology. (b) Measured dielectric permittivity response under applied dc-electric fields at 1 kHz. (c) Room temperature ferroelectric hysteresis response for the various compositions measured at 1 kHz. (d) Current−voltage response for the various compositions measured on 6.2×10^{-5} cm^2 device areas.

have addressed the evolution of pyroelectric responses at such features.[10−13]

Therefore, future work must address the lack of in-depth understanding of the various contributions to pyroelectric response, how and why π varies in magnitude and sign with material chemistry, strain, etc. and, in turn, what can be done outside tuning T_C to produce large pyroelectric effects near room temperature. Such a discussion requires that we understand the potential contributions to pyroelectric response. In general, one may express the total pyroelectric response as

$$\begin{aligned}\pi &= \pi_{\text{Int}} + \pi_{\text{Ext}} + \pi_{\text{Sec}} + \pi_{\varepsilon} + \pi_{\text{Ter}} \\ &= \phi\left(\frac{\partial P_s}{\partial T}\right)_x + P_s\left(\frac{\partial \phi}{\partial T}\right)_x + \left(\frac{\partial P_s}{\partial X}\right)_T\left(\frac{\partial X}{\partial x}\right)_T\left(\frac{\partial x}{\partial T}\right)_X + \varepsilon_0 E\left(\frac{\partial \varepsilon_r(E)}{\partial T}\right) + \pi_{\text{Ter}}\end{aligned} \quad (2)$$

where ϕ is the fraction of ferroelectric domains contributing to the pyroelectric response, x is the strain, ε_0 is the permittivity of free space, and ε_r is the relative permittivity. Here, the primary contribution is defined by the combination of both the intrinsic (π_{Int}, first term) and extrinsic (π_{Ext}, second term) effects, similar to that of dielectrics.[14−16] The intrinsic contribution arises from the temperature dependence of P_s (i.e., within the ferroelectric domains), while the extrinsic contribution arises from the temperature dependence of the domain structure (i.e., thermally induced domain-wall motion).[14] The secondary contribution (π_{Sec}, third term), in general, arises from the fact that all pyroelectric materials are also piezoelectric. Thus, temperature-induced volume changes are commensurate with piezoelectric polarization changes. Furthermore, complications arise in thin-film geometries where the thermal-expansion mismatch between the film and substrate provides additional induced stress by confining the free in-plane thermal expansion of the film, and thus can induce additional changes in P_s via the piezoelectric effect. To encompass all these coupled subtleties, the secondary contribution includes material properties such as the piezoelectric coefficient, elastic stiffness, and the thermal-expansion coefficient.[14,17,18] Furthermore, under applied electric fields, a dielectric contribution (π_{ε}, fourth term) arises from the temperature and electric-field dependence of ε_r. Lastly, the tertiary contribution (π_{Ter}, fifth term) arises via the piezoelectric effect from inhomogeneous heating that induces nonuniform stresses.[19] This effect typically only pertains to bulk materials and may be neglected if uniform heating is achieved; which is typically the case in thin films. To date, outside of a limited number of phenomenological-modeling treatments[14,15,20] and indirect-property measurements,[21] there have been few attempts to directly extract these various contributions to electrothermal response.[22,23]

Here, combining thin-film epitaxy, extensive field- and temperature-dependent property measurements, including direct electrothermal measurements of pyroelectric currents in thin-film capacitors, we extract and quantify the intrinsic, extrinsic, dielectric, and secondary pyroelectric contributions to pyroelectricity in $PbZr_{1-x}Ti_xO_3$ (x = 0.40, 0.48, 0.60, and 0.80) as a function of chemistry across the MPB. Using phase-sensitive frequency and field-dependent electrothermal measurements, it is possible to independently suppress (i.e., turn-off) the secondary, extrinsic, and dielectric contributions to elucidate the magnitude and sign of all contributions to the overall response. The total pyroelectric response decreases systematically as one moves from higher to lower titanium contents as a result of a combination of decreasing intrinsic response and a sign inversion of the extrinsic contribution upon crossing the MPB. The intrinsic response can range from −232 to −97 $\mu C\ m^{-2}\ K^{-1}$, in some cases closely approaching the total measured response. The extrinsic response varies greatly in magnitude and sign as the chemistry is varied (from +33 to −17 $\mu C\ m^{-2}\ K^{-1}$) and can thus dramatically reduce the total pyroelectric response in some cases. The secondary contribution spans between −70 to −29 $\mu C\ m^{-2}\ K^{-1}$ and

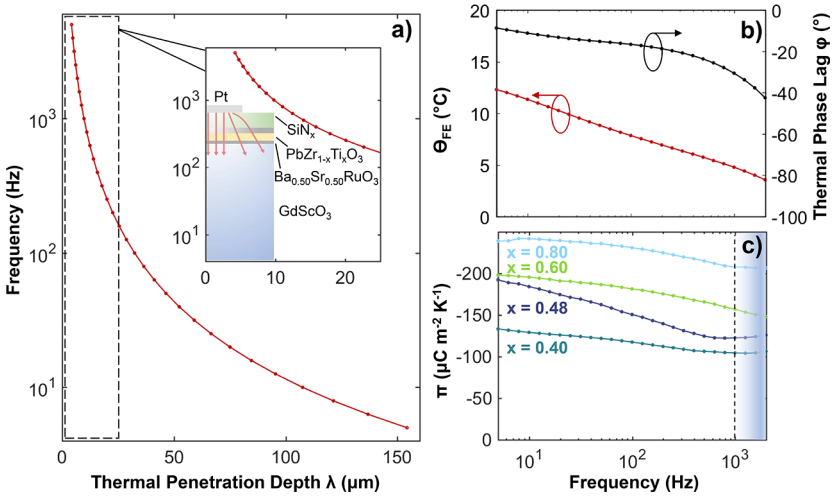

Figure 2. Thermal and secondary measurements of $PbZr_{1-x}Ti_xO_3$ thin-films.(a) Calculated thermal penetration depth into the $GdScO_3$ substrate used to define the cutoff frequency for secondary contributions. Inset displays a schematic of the heat flux through the thin-film stack where the heater half width is approached at 1 kHz. (b) Temperature oscillation amplitude (left axis) and associated thermal phase lag (right axis) within the ferroelectric film as a function of heating frequency 1ω. (c) Frequency dependence of the π displaying a suppressed secondary effect past ~1 kHz.

scales directly with the piezoelectric response of the materials and the dielectric contribution can be varied from 10 to 115 $\mu C\ m^{-2}\ K^{-1}$ (at E = 100 kV cm^{-1}), following trends in the dielectric susceptibility. Regardless of chemistry, under zero applied field the intrinsic contribution (56−99%) is found to provide the largest component of overall response followed by the secondary (15−35%) and extrinsic (2−14%) effects. Under applied fields, the dielectric effects can also be large (4−58% at the largest measured total response). These findings and the methodologies developed to extract them provide novel insights into the understudied realm of pyroelectric response.

RESULTS AND DISCUSSION

In order to systematically investigate the various pyroelectric contributions as one transitions across the MPB, a composition series of 100−140 nm-thick $PbZr_{0.60}Ti_{0.40}O_3$, $PbZr_{0.52}Ti_{0.48}O_3$, $PbZr_{0.40}Ti_{0.60}O_3$, and $PbZr_{0.2}Ti_{0.8}O_3$ thin films (henceforth referred to as x = 0.40, 0.48, 0.60, and 0.80 heterostructures, respectively), were grown on 20 nm $Ba_{0.50}Sr_{0.50}RuO_3/GdScO_3$ (110) single-crystal substrates via pulsed-laser deposition (Materials and Methods).[24] We note that the 120 nm-thick x = 0.80 heterostructures were used in a prior study and are included here for additional comparison and to validate the overall measurements and direct extraction methodologies developed herein.[25] θ-2θ X-ray diffraction and atomic force microscopy studies (Figure 1a, Materials and Methods, and Supporting Information, Figure S1) confirm that, in all cases, the heterostructures are single-phase, epitaxial, and of high surface topography quality (root-mean-square roughness <600 pm). Due to the relatively large lattice mismatch (1−3%) between the films and the underlying substrates, all heterostructures were found to be grown in a relaxed-strain state from reciprocal space mapping studies (Supporting Information, Figure S1c−e). Preliminary X-ray diffraction, dielectric, and ferroelectric studies for the x = 0.80 heterostructures are reported elsewhere.[25] In total, we have a systematic set of $PbZr_{1-x}Ti_xO_3$ films varying only in chemistry that can be used to probe the evolution of pyroelectric response.

Following structural studies, the electrothermal devices were fabricated (Materials and Methods)[22,25] and were then used to probe the evolution of dielectric, ferroelectric, and pyroelectric properties (Materials and Methods). First, the dielectric permittivity as a function of background dc bias (for brevity shown at 1 kHz), further confirms the quality of the heterostructures and begins to provide insight into the variations in material response (Figure 1b). The dielectric permittivity is expected, and is measured, to be the largest in heterostructures with MPB chemistry (x = 0.48) and then to drop off, first to the x = 0.40 heterostructures (with rhombohedral structure) and then to the x = 0.60 heterostructures (with tetragonal structure).[6] Likewise, as expected, the x = 0.48 heterostructures also showed the largest dielectric tunability (~69% at 300 kV cm^{-2}). It is noted that all heterostructure variants displayed low loss-tangent values across the same electric-field regime (<0.1; Supporting Information, Figure S2). Additionally, polarization-electric-field hysteresis loops (again, for brevity, reported at 1 kHz) were measured and, as expected, the largest P_s values were observed for the x = 0.60 heterostructures, while the x = 0.48 heterostructures exhibited the lowest (Figure 1c). The insulating properties of these thin films were further confirmed via studies of current density with applied dc voltage (i.e., leakage studies), where symmetric response with low-leakage currents (<10^{-2} A cm^{-2}), that improve with increasing zirconium content, were observed (Figure 1d). In all, the $PbZr_{1-x}Ti_xO_3$ composition series exhibits the crystal structure and dielectric and ferroelectric properties we desire and which are consistent with previous reports.[26]

Armed with this set of high-quality heterostructures, we proceeded to explore the evolution of the pyroelectric response. As previously defined, the secondary contribution to pyroelectricity in thin films arises from the elastic-boundary conditions of the substrate that confines the in-plane thermal expansion of the film, and thus induces a stress that drives a piezoelectric response. With the thin (100 nm) platinum resistive heater geometry used in this work, a characteristic thermal-penetration depth (λ) into the $GdScO_3$ substrate may be expressed as

$$\lambda = \sqrt{\frac{D}{2\omega}} \tag{3}$$

where D and ω refer to the thermal diffusivity ($m^2\ s^{-1}$) and heating current oscillation angular frequency (rad s^{-1}), respectively.[27] By adjusting the angular frequency of the input heating current $I_{1\omega}$ to the resistive line, we are able to control the λ between approximately 5−150 μm (Figure 2a). In turn, by investigating the frequency response of λ, it is possible to identify two regimes of response. At low frequencies (<10 Hz), ∼30% of the total substrate thickness (500 μm) is effectively being heated, allowing for local thermal expansion of the substrate, and thus a secondary contribution from thermal expansion mismatch with the heated film. At high frequencies (>1 kHz), however, λ becomes comparable to the half-heater width (5 μm), and only ∼1% of the substrate thickness is heated. This small heated fraction of the total substrate thickness is clamped by the surrounding ∼99% of unheated substrate and thus has negligible thermal expansion. Within this regime, both the in-plane thermal expansion of the semi-infinite substrate and, in turn, secondary contribution in the system are effectively suppressed.[28] By limiting λ to a negligible fraction of the substrate, we have identified a route to obtain negligible secondary contributions (inset, Figure 2a).

To quantitatively estimate the frequency cutoff regime for the secondary contribution, the peak-to-peak sinusoidal temperature oscillation amplitude of the ferroelectric θ_{FE} ($°C_{pk\text{-}pk}$) and the thermal-phase lag to the input heating current $I_{1\omega}$ were characterized (Figure 2b).[22] From this, the total π could be calculated as a function of heating input frequency (Figure 2c). As the frequency of the measurement is increased, π decreases and begins to flatten out at ∼1 kHz, indicative of a suppression of the secondary contribution.[28] There are two important observations to be made from this data. First, as the titanium content (x) decreases, so does the overall π (from −242 to −129 $\mu C\ m^{-2}\ K^{-1}$ at 10 Hz for x = 0.8 and 0.4 heterostructures, respectively). Second, this trend remains even when the secondary contribution is suppressed at high frequency. Subtracting the total π at 1 kHz from that at 10 Hz to extract the effective secondary contribution in this frequency range, we see a reduction of magnitude of 29, 70, 41, and 34 $\mu C\ m^{-2}\ K^{-1}$ for the x = 0.40, 0.48, 0.60, and 0.80 heterostructures, respectively. We note that this effective secondary contribution is specific only to this frequency regime (i.e., it could be slightly larger in some cases) since full saturation of π at low frequencies is limited by the noise floor of the collected pyroelectric current (i_p). The greatest secondary contributions are found closer to the MPB, consistent with the expected enhanced effective piezoelectric coefficient d^*_{jkl} in those materials. Due to the systematic use of $GdScO_3$ substrates (i.e., an equivalent elastic-boundary condition across all heterostructure compositions), differences in secondary response may be primarily attributed to varying piezoelectric responses. In total, it is possible to identify frequency regimes where secondary effects may be effectively suppressed, thus providing experimental boundaries for the following electrothermal measurements.

Having effectively shown that we can suppress (and therefore quantify) the secondary contribution, our attention shifted to understanding the dielectric and extrinsic contributions. Again, the extrinsic contribution refers to the temperature-dependent change in the domain structure whereby a change in temperature induces domain-wall motion as more temperature-stable domain structures grow at the expense of less stable structures.[15] Similar to the contribution domain structure plays in piezoelectric and dielectric susceptibilities,[29] extrinsic effects can comprise a large percentage (>35%) of the total pyroelectric response,[25] and thus are an essential contribution to understand and control. In the study of dielectric response, there are various approaches that have been demonstrated to separate out extrinsic effects. One, for example, aims to suppress domain-wall motion, and thus extrinsic contributions, via low-temperature measurements. Prior work[29] focused on low temperature (∼5 K) ac electric-field studies to elucidate the contributions and suppression of extrinsic effects where domain-wall motion is no longer thermally activated. Another approach aims to suppress domain-wall motion via high applied dc-electric fields. Prior work on $PbZr_{1-x}Ti_xO_3$ thin films identified dc-field regimes >200 kV cm^{-1} wherein domain walls become electrically "pinned", thus suppressing extrinsic contributions and diminishing the overall dielectric response.[30,31]To date, no equivalent methodologies have been developed for pyroelectric response.

As such, we initially explored analogous approaches. First, focusing on low-temperature studies, a clear suppression of the total i_p response was found as expected; however, extraction of π via eq 5 (Materials and Methods) remained challenging due to the reduced temperature dependence of the platinum-heater-line resistance and associated dc temperature rises at temperatures <20 K (i.e., where domain-wall motion is suppressed). In turn, the applied ac-temperature oscillations and material dc temperature could not be accurately characterized and easily controlled in the thin-film 3ω method applied herein.[27,32] Based on this observation, we turned to high-dc-bias techniques to attempt to suppress domain-wall contributions. From a naïve point of view, simply completing pyroelectric studies as a function of dc bias should provide a way to quench (at high biases) the extrinsic contributions. While this is true, it is also convoluted with any potential dielectric contributions that arise from applied bias. To separate out these two effects, we recall that the dielectric contribution is defined as $\varepsilon_0 E\left(\frac{\partial \varepsilon_r(E)}{\partial T}\right)$ and requires knowledge of both the field and temperature dependence of ε_r (Figure 3a). To obtain this information, we measured the capacitance as a function of field (E = 0−500 kV cm^{-1}) at three temperatures (i.e., 23, 33, and 42 °C; Figure 3b) and extracted the derivative of the curve in the temperature regime of interest (Materials and Methods, Figure 3c). Such data for the x = 0.40, 0.48, 0.60, and 0.80 heterostructures reveals that all compositions experience a reduction of permittivity with increasing bias which is explained via the suppression of the extrinsic domain-wall contributions at high fields (Figure 3b).[23] Within a temperature regime similar to that applied for the pyroelectric studies (ΔT = 19 °C), the largest dispersion in permittivity is found at lower fields (for brevity, representative data for the x = 0.48 heterostructures is provided; inset, Figure 3b). In turn, we can extract values of $\frac{\partial \varepsilon_r(E)}{\partial T}$ for the various heterostructures as a function of dc bias (Figure 3c) to be used to quantify the dielectric contribution to pyroelectricity. Due to enhanced dielectric susceptibility, the x = 0.48 heterostructures are found to have the highest dielectric contribution to pyroelectricity, followed first by the x = 0.40, and then the x = 0.60 and 0.80 heterostructures—following the trend in overall dielectric permittivity. Additionally, all dielectric contributions begin to asymptotically approach 0 K^{-1} past ∼300 kV cm^{-1}. Thus, by taking the derivative $\frac{\partial \varepsilon_r(E)}{\partial T}$ at each given applied dc

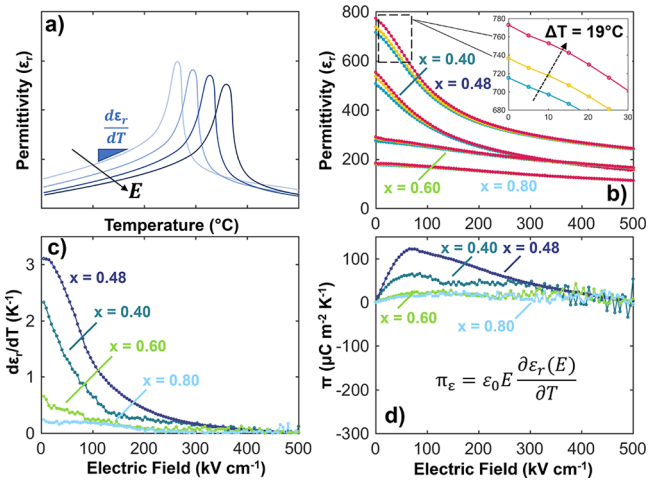

Figure 3. Extraction of the dielectric contribution to π. (a) Prototypical temperature dependence of the dielectric permittivity under applied dc-electric (E) fields. (b) Summary of the temperature dependent (23, 33, and 42 °C) ε_r results as a function of applied dc-electric field for all heterostructures (Inset displays magnified results at low fields for x = 0.48). (c) Extracted temperature derivative of ε_r as a function of applied dc bias for the various heterostructures. (d) Calculated *dielectric* contributions as a function of field (i.e., $\pi_e = \varepsilon_0 E \frac{\partial \varepsilon_r(E)}{\partial T}$) for all heterostructures; note all start at zero at zero applied field.

field, and multiplying by $\varepsilon_0 E$, the total dielectric contribution may be extracted as a function of field (Figure 3d). As such, the dielectric contribution begins at 0 μC m^{-2} K^{-1} when there is no applied electric field [since $\left(\varepsilon_0 E \frac{\partial \varepsilon_r(E)}{\partial T}\right)$], rises at intermediate fields, and finally decreases toward zero at higher fields as $\frac{\partial \varepsilon_r(E)}{\partial T}$ is suppressed. Thus, by simply obtaining the temperature dependence of the dielectric permittivity under various applied dc biases, one can quantify (and subtract) this dielectric contribution (π_e).

Bringing this all together, we can complete dc-bias-dependent pyroelectric measurements in such a fashion that it allows us to account for the various contributions. First, the secondary contribution can be obtained by completing the measurements as a function of frequency and comparing the results at low (i.e., ~10 Hz) and high (i.e., ~1 kHz) frequency where the secondary contribution is quenched. Second, dc-bias dependence provides us the ability to quench the extrinsic contribution at high dc biases. Finally, the additional field- and temperature-dependent studies of ε_r noted above (Figure 3) allow us to quantify and decouple the dielectric contribution induced by the applied bias. The dc-bias evolution of i_p for the various heterostructures is provided, shown here scaled to the heater powers used for the x = 0.80 and 0.60 heterostructures to enable direct comparison (Figure 4a). All heterostructure variants display a characteristic i_p hysteresis loop, indicating two oppositely poled polarization states. In turn, the total π can then be extracted as a function of dc bias (note that π values are negative), and, again, a decrease in the maximum π is observed as the titanium content (x) is decreased (Figure 4b). Similar to previous reports,[25,33] a butterfly-like response is observed, where the minima in pyroelectric response occur at the coercive field. Evidence of the dielectric contribution is observed in the positive slope of the total π as the magnitude of the applied electric field is increased. Due to the fact that $\frac{\partial \varepsilon_r(E)}{\partial T}$ remains intrinsically positive below T_C (Figure 3a), this contribution opposes the overall negative π values.

With the secondary and dielectric contributions quantified, attention was next directed toward extracting the intrinsic response. Similar to intrinsic contribution extraction methodologies in dielectrics,[30,31] we utilized high-field π response to fit and extract the zero-field intrinsic contribution. Specifically, by extending the field-dependent pyroelectric response studies (Figure 4b) to higher dc-electric fields (500 kV cm^{-1}), the dielectric and extrinsic contributions can be effectively suppressed. Following the approach used in dielectric studies, we can then extrapolate back to zero bias to extract the zero-bias intrinsic response. Using the slope of π from the high-field regime (i.e., 450−500 kV cm^{-1}), we extrapolate linear response to zero field for the various compositions (Figure 4c). All heterostructure variants exhibit a nearly field independent intrinsic response (slope α_i), similarly seen to the intrinsic contribution extraction for dielectric response.[30,31] Specifically, zero-field intrinsic values (π_{Int}) of −220, −179, −110, and −97 μC m^{-2} K^{-1} are extracted for the x = 0.80, 0.60, 0.48, and 0.40 heterostructures, respectively. Here we see a decreasing contribution to the overall response with decreasing titanium composition (x); consistent with previous phenomenological predictions.[14]

To begin to explain the total composition dependence of π, a detailed methodology of contribution extraction is demonstrated, as an example, on the x = 0.80 heterostructures which were previously characterized using a monodomain (i.e., zero extrinsic contribution) reference sample.[25] Namely, using

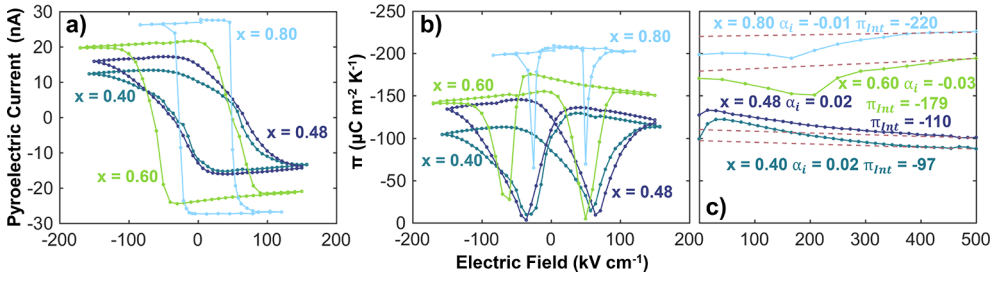

Figure 4. Pyroelectric and intrinsic DC field dependence of $PbZr_{1-x}Ti_xO_3$ heterostructures. (a) Applied dc-electric-field response of room temperature pyroelectric currents measured at 1 kHz and 10 mA rms heating current. Heating powers for x = 0.40 and 0.48 are scaled to the applied power used for the x = 0.60 and 0.80 heterostructures due to different heater-line resistances. (b) Pyroelectric coefficient results under applied dc bias for the various compositions measured at 1 kHz. (c) Intrinsic contribution extraction and dc-electric-field dependence from high-field π. Here, α_i and π_{int} refer to the slope and zero-field value of the field-dependent intrinsic contribution.

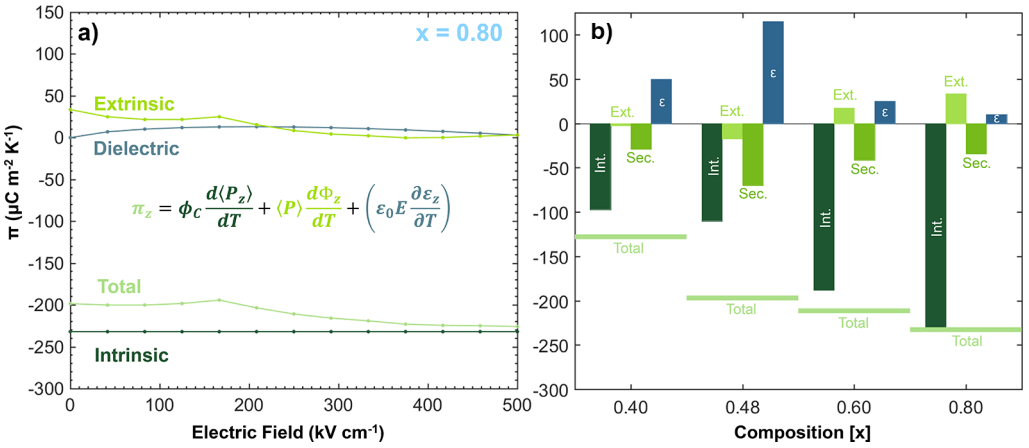

Figure 5. Extraction of the various contributions to π for $PbZr_{1-x}Ti_xO_3$ heterostructures.(a) dc-field dependence of the total π and extracted extrinsic, dielectric, and intrinsic π contributions for x = 0.80 heterostructures. (b) Summary of the intrinsic, extrinsic, secondary, and total π response as a function of composition across the various $PbZr_{1-x}Ti_xO_3$ chemistries studied herein. Due to the opposing signs of the various contributions, the total net π value is indicated via a solid line for each composition. The dielectric contribution displayed here is that measured at an applied dc-electric field of 100 kV cm^{-1}.

the measured total (Figure 4b), intrinsic (Figure 4c), dielectric (Figure 3d), and secondary (Figure 2c) contributions, the extrinsic contribution can be solved for in a self-consistent fashion according to eq 2. Again, the secondary contribution can be quenched by operating at high frequencies (1 kHz) thus allowing direct quantification of this value. The intrinsic contribution can then be extracted from the zero-field intercept of a line with the slope of the high-field total pyroelectric response (similar to approaches used in dielectrics[30]). The measured dielectric response is extracted from $C-V$ methodologies and is zero at zero field. Likewise, the extrinsic contribution should approach 0 μC m^{-2} K^{-1} at high fields as we quench domain-wall motion. Armed with this evolution, we can self-consistently solve for the extrinsic contribution to the total response. Specifically, using the full-range (i.e., 0−500 kV cm^{-1}) dc-bias dependence of the total π we can identify where the extrinsic response asymptotes to 0 μC m^{-2} K^{-1} such that it fulfills the conditions above. For the x = 0.80 heterostructures, the extrinsic response is found to approach zero near 300 kV cm^{-1} (Figure 5a). Again, to quantify the extrinsic contribution from eq 2, the response is extracted at 1 kHz and zero field, where secondary and dielectric contributions can be excluded. Compared to recent work,[25] the intrinsic (~-250 μC m^{-2} K^{-1}) and extrinsic (~40 μC m^{-2} K^{-1}) values align quite closely at E = 0 kV cm^{-1}; thus confirming the validity of this methodology. Due to the ac nature of the pyroelectric measurements, dc-leakage currents induced by applied dc biases do not contribute to the collected i_p. The major advantage of this proposed methodology is that it allows researchers to extract extrinsic contributions without the need for free-standing geometries, intricate knowledge of piezoelectric/thermal properties, and/or monodomain-reference samples (something that may not be possible to achieve for all ferroelectric systems).[25,34−36]

Applying the same methodology to the other compositions (Supporting Information, Figure S3), a comprehensive comparison of all π contributions may be made (Figure 5b). Here, both the total and intrinsic contributions display decreasing values as the titanium content (x) is decreased. This trend may be explained, in part, via the intrinsic polarization axis moving away from the out-of-plane [001] for the titanium-rich, tetragonal phases toward the [111] for the titanium-poor, rhombohedral phases, thus contributing less to the out-of-plane total measured response. Furthermore, the secondary contribution not only depends on the thermal-expansion mismatch between the film and substrate, but additionally on the piezoelectric coefficient d^*_{jkl} of the film. Due to the use of $GdScO_3$ substrates across all compositions, the systematic increase and maximum of the secondary contribution in proximity to the MPB is thus attributed to the enhanced piezoelectric susceptibility since the thermal expansion mismatch is not expected to vary greatly.[14,37,38] Following previous phenomenological models,[14] the extrinsic contribution does decrease as one approaches the MPB from the titanium-rich side and actually undergoes a sign inversion upon proceeding to the zirconium-rich side of the phase diagram and is explained by changes in how the domain structures respond to temperature changes in this regime. Unlike the case for $BaTiO_3$ and titanium-rich $PbZr_{1-x}Ti_xO_3$ where abundant strain-dependent phase diagrams provide insight into the thermodynamic stability of domain phases,[39,40] there has been less attention on the zirconium-rich side of the phase diagram. Titanium-rich compositions are known to exhibit an increase in c-domain fraction upon heating at compressive strains (i.e., positive extrinsic contribution),[39] however, this appears to be the opposite for these relaxed zirconium-rich heterostructures. Due to the curvature of the monoclinic phase toward the zirconium-rich compositions and the polar axis remaining in the plane between the [001] and [111], compositions at or near the monoclinic phase of $PbZr_{1-x}Ti_xO_3$ would be expected to have a decrease in out-of-plane polarized domains as the rhombohedral phase is approached.[41−43] Therefore, the $\left(\frac{\partial \phi}{\partial T}\right)$ term would in fact be negative as decreased out-of-plane polarizations are stabilized upon heating, thus directly supporting the total negative pyroelectric response. Naïvely speaking, one would predict that an enhanced negative extrinsic contribution would drive an overall higher magnitude π response, however, with our ability to quantify the intrinsic and other contributions, it is clear this is not always the case. For titanium-rich compositions, large dominating intrinsic values work against extrinsic contributions that are of the opposite sign. Upon crossing the MPB, even

though the sign of the extrinsic contribution changes to work together with the intrinsic response, this coincides with a strong reduction in the intrinsic response arising from a symmetry change in the material. The result is a diminished overall response. In order to maximize the total pyroelectric response in the $PbZr_{1-x}Ti_xO_3$ system, a minimally strained (<−0.25%) tetragonal thin film of composition $x = 0.80$ could be developed to minimize the counteracting positive extrinsic response, while maintaining enhanced intrinsic contributions relative to the cases where diminished intrinsic response follows extrinsic sign inversions. The key to pyroelectric susceptibility enhancement lies in the ability to control intrinsic and extrinsic contributions via composition and elastic boundary conditions, respectively.

CONCLUSION

In total, frequency and dc-bias methodologies have been applied to systematically investigate and directly extract numerous pyroelectric contributions as a function of chemistry across the MPB of the $PbZr_{1-x}Ti_xO_3$ system. Unlike dielectric and piezoelectric susceptibilities which are found to become maximum at the MPB, the pyroelectric response displays a systematic reduction as the titanium content (x) is decreased. This reduction is explained primarily via the reduction of the intrinsic pyroelectric contribution, in which the out-of-plane polar axis component is reduced upon transitioning from the tetragonal to the rhombohedral side of the phase diagram. Additionally, an inversion of the sign of the extrinsic contribution was found to lie in the vicinity of the MPB in which the temperature dependence of the out-of-plane pointing domain fractions decreases upon heating. In all, the intrinsic response accounted for upward of 99% (|97−232| μC m^{-2} K^{-1}) of the total measured pyroelectric response, while the extrinsic and secondary contributions account for ∼8% (|2−33| μC m^{-2} K^{-1}) and ∼23% (|29−70| μC m^{-2} K^{-1}), respectively. Additionally, following trends in the dielectric susceptibility, the measured dielectric contribution ranged from |10−115| μC m^{-2} K^{-1} at an applied electric field of 100 kV cm^{-1} for the respective compositions. This work has not only provided the community with a comprehensive pyroelectric extraction methodology, but elucidated the need to directly characterize and consider all pyroelectric contributions of ferroelectric systems for the thoughtful design of enhanced susceptibility within pyroelectric materials.

MATERIALS AND METHODS

Film Growth and Structural Characterization. In order to systematically investigate the various pyroelectric contributions as one transitions across the MPB, a composition series of 100−140 nm-thick $PbZr_{0.60}Ti_{0.40}O_3$, $PbZr_{0.52}Ti_{0.48}O_3$, $PbZr_{0.40}Ti_{0.60}O_3$, and $PbZr_{0.2}Ti_{0.8}O_3$ thin films (henceforth referred to as $x = 0.40$, 0.48, 0.60, and 0.80 heterostructures, respectively), were grown on 20 nm $Ba_{0.50}Sr_{0.50}RuO_3/GdScO_3$ (110) single-crystal substrates via pulsed-laser deposition in an on-axis geometry (target to substrate spacing of 5.2 cm).[24] We note that the 120 nm-thick $x = 0.80$ heterostructures were used in a prior study and are included here for additional comparison and to validate the overall measurements and direct extraction methodologies developed herein.[25] Using a KrF excimer laser (Coherent LPX-300, λ = 248 nm), 20 nm $Ba_{0.50}Sr_{0.50}RuO_3$ bottom electrodes were deposited from a ceramic target of the same chemistry at a heater temperature of 700 °C in a dynamic oxygen-partial pressure of 100 mTorr and laser fluence of 1.13 J cm^{-2} (10 Hz laser repetition rate). Following the growth of the $Ba_{0.50}Sr_{0.50}RuO_3$, the $PbZr_{1-x}Ti_xO_3$ films were deposited from ceramic targets of the various chemistries noted with 10% lead excess at a heater temperature of 610 °C, in a dynamic oxygen-partial pressure of 100 mTorr and a laser fluence of 0.83 J cm^{-2} (10 Hz laser repetition rate). As the growth rates from the different targets vary, thickness calibrations were completed using X-ray reflectivity to ensure films of similar thickness were produced (Supporting Information, Figure S1a). Following growth of the $PbZr_{1-x}Ti_xO_3$ films, 40 nm $Ba_{0.50}Sr_{0.50}RuO_3$ top electrodes were deposited from a ceramic target of the same chemistry at a heater temperature of 610 °C, keeping all other growth parameters consistent with the bottom electrode deposition. Following growth of all layers, the heterostructures were cooled to room temperature in a static oxygen pressure of ∼700 Torr at a rate of 5 °C min^{-1}. Following growth, all films were subjected to extensive structural characterization including X-ray θ-2θ line scans, reciprocal space mapping studies (Supporting Information, Figure S1b-d), and X-ray reflectivity measurements using Cu Kα radiation (Panalytical X'Pert 3 MRD diffractometer). Lastly, representative bilayer structures (i.e., without top electrodes) were grown under the aforementioned conditions to allow surface morphology studies of the $PbZr_{1-x}Ti_xO_3$ using atomic force microscopy (Asylum Research, MFP-3D).

Electrothermal Device Fabrication. Following previously defined processing methods,[22,25] the development of the electrothermal test platforms used in this work is briefly summarized here. With the trilayer capacitor structures noted above, the active device regions were defined via photolithography and ion milling. The top and bottom electrodes were further ion milled to isolate their overlay solely within the active device strip. Following this, a 200 nm-thick blanket layer of SiN_x was deposited via plasma-enhanced chemical vapor deposition (SiH_4 + NH_3 at 350 °C and 950 mTorr) to isolate the electrical capacitor circuit from the overlying heating circuit. The blanket layer SiN_x was further defined into the appropriate configuration to separate it from the top heater circuit via reactive-ion etching with O_2 and CHF_3 gases under 250 W of RF power. Lastly, a 100 nm-thick platinum resistive heater line was sputtered at room temperature under an argon-partial pressure of 7 mTorr to define the top thermal circuit.

Dielectric, Ferroelectric, and Pyroelectric Characterization. All polarization-electric field hysteresis loops and current−voltage response were acquired using a ferroelectric tester (Radiant Technologies, Precision Multiferroic Tester), where triangular and linear voltage waveforms wereapplied at various frequencies across the ferroelectric capacitor structure. Extraction of dielectric properties was acquired with an impedance analyzer (Keysight E4990A) wherein a 10 mA ac sensing signal was used to extract the capacitance and loss tangent as a function of applied dc voltage (C−V). Furthermore, in order to capture the temperature dependence of $\varepsilon_r(E)$ necessary to extract the *dielectric* contribution $\left(\varepsilon_0 E\frac{\partial \varepsilon_r(E)}{\partial T}\right)$, prepoled, monopolar C−V measurements were completed up to E = 500 kV cm^{-1} at three temperatures (i.e., 23, 33, and 42 °C). Due to the relatively high T_C for this system(>400 °C),[27] nonlinearity of $\varepsilon_r(E)$ may be neglected within the near-room-temperature regime chosen for this study. Finally, linear fits $\left(\frac{\partial \varepsilon_r(E)}{\partial T}\right)$ were extracted for each electric field to calculate the final dielectric contribution.

Direct ac pyroelectric characterization following established processes[22,25] was completed and is summarized briefly here. A resistive heating current [$I_{1\omega} = I_0 \cos(\omega t)$] was applied to the top platinum line via a current source (Keithley 6221) at 10 mA rms amplitude to produce temperature oscillations via Joule heating ($P = I^2R$). The oscillating temperature amplitude (2ω) results in an oscillating heater-line resistance at 2ω. With the input heating current (1ω) multiplied with the heater resistance (2ω), the third harmonic (3ω) of the voltage drop across the line could be measured (3ω method)[27,32] via a lock-in amplifier (SRS SR830). With the 3ω voltage response characterized; the average heater temperature amplitude may be expressed as

$$\theta_0 = 2\frac{V_{3\omega}}{R_0 I_0 \alpha} \quad (4)$$

where α refers to the temperature coefficient of resistance of the platinum $\left(\alpha = \frac{dR}{dT}\frac{1}{R_0}\right)$. With known applied temperature oscillations and the effective electrode area (A), π may be extracted from the measured pyroelectric current (i_p) as[1]

$$i_p = \pi A \frac{dT}{dt} \quad (5)$$

Careful consideration of phase sensitivity was taken to ensure that the collected i_p was purely 90° out-of-phase with the input temperature oscillation. This step allows one to confidently separate out spurious, thermally stimulated currents that can plague nonphase-sensitive measurements.[44−46]

AUTHOR INFORMATION

Corresponding Author

*E-mail: lwmartin@berkeley.edu.

ORCID

Gabriel Velarde: 0000-0002-7389-2017

Lei Zhang: 0000-0002-1559-8469

Lane W. Martin: 0000-0003-1889-2513

Author Contributions

G.V., S.P., and L.W.M. conceived of the core concepts and designed the experiments. R.G., E.L., D.G., and S.P. synthesized and or aided in the synthesis the various thin-films. G.V. fabricated the electrothermal devices and performed the dielectric, ferroelectric, and pyroelectric measurements. J.W. contributed to implementing the heat transport models. G.V. and L.Z. contributed to the analysis, discussions, understanding of the data and the development of the manuscript. G.V. and L.W.M. wrote the core of the manuscript. All authors discussed the results and the implications of the work and commented on the manuscript at all stages.

Notes

The authors declare no competing financial interest.

ACKNOWLEDGMENTS

G.V. acknowledges support from the National Science Foundation under Grant DMR-1708615. S.P. acknowledges support from the Army Research Office under Grant W911NF-14-1-0104. L.Z. acknowledges support from the U.S. Department of Energy, Office of Science, Office of Basic Energy Sciences, under Award Number DE-SC-0012375 for the study of ferroelectric thin films. J.D.W. acknowledges support from an NSF Graduate Research Fellowship under Grant No. DGE 1752814. L.W.M. acknowledges partial support from the U.S. Department of Energy, Office of Science, Office of Basic Energy Sciences, Materials Sciences and Engineering Division under Contract No. DE-AC02-05-CH11231, Materials Project program KC23MP for the development and study of novel functional materials.

REFERENCES

(1) Jachalke, A.; Mehner, E.; Stocker, H.; Hanzig, J.; Sonntag, M.; Weigel, T.; Leisegang, T.; Meyer, D. C. How to Measure the Pyroelectric Coefficient? *Appl. Phys. Rev.* **2017**, *4*, 021303.

(2) Lines, M. E.; Glass, A. M. *Principles and Applications of Ferroelectrics and Related Materials*; Oxford University Press: New York, 1977.

(3) Whatmore, R. W. Pyroelectric Devices and Materials. *Rep. Prog. Phys.* **1986**, *49*, 1335−1386.

(4) Hadni, A. Applications of the Pyroelectric Effect. *J. Phys. E: Sci. Instrum.* **1981**, *14*, 1233−1240.

(5) Mischenko, A. S.; Zhang, Q.; Scott, J. F.; Whatmore, R. W.; Mathur, N. D. Giant Electrocaloric Effect in the Thin Film Relaxor Ferroelectric 0.9PbMg$_{1/3}$Nb$_{2/3}$O$_3$-0.1PbTiO$_3$Near Room Temperature. *Science* **2006**, *311*, 1270−1271.

(6) Damjanovic, D. Comments on Origins of Enhanced Piezoelectric Properties in Ferroelectrics. *IEEE Trans. Ultrason. Ferroelectr. Freq. Control.* **2009**, *56*, 1574−1585.

(7) Fu, H.; Cohen, R. E. Polarization Rotation Mechanism for Ultrahigh Electromechanical Response in Single-Crystal Piezoelectrics. *Nature* **2000**, *403*, 281−283.

(8) Noheda, B.; Cox, D. E.; Shirane, G.; Park, S.-E.; Cross, L. E.; Zhong, Z. Polarization Rotation via a Monoclinic Phase in the Piezoelectric 92%PbZn$_{1/3}$Nb$_{2/3}$O$_3$-8%PbTiO$_3$. *Phys. Rev. Lett.* **2001**, *86*, 3891−3894.

(9) Damjanovic, D. A Morphotropic Phase Boundary System Based on Polarization Rotation and Polarization Extension. *Appl. Phys. Lett.* **2010**, *97*, 062906.

(10) Teowee, G.; McCarthy, F. S.; McCarthy, K. C.; Dietz, B. H.; Uhlmann, D. R. Pyroelectric Properties of Sol-Gel Derived PZTThin Films with Various Zr/TiRatios. *Integr. Ferroelectr.* **1998**, *22*, 431−438.

(11) Yang, J.-S.; Kim, S.-H.; Yeom, J.-H.; Koo, C.-Y.; Hwang, C. S.; Yoon, E.; Kim, D.-J.; Ha, J. Piezoelectric and Pyroelectric Properties of Pb(Zr,Ti)O$_3$Films for Micro-Sensors and Actuators. *Integr. Ferroelectr.* **2003**, *54*, 515−525.

(12) Xiao, B.; Avrutin, V.; Liu, H.; Ozugur, U.; Morkoc, H.; Lu, C. Large Pyroelectric Effect in Undoped Epitaxial Pb(Zr,Ti)O$_3$Thin Films on SrTiO$_3$ Substrates. *Appl. Phys. Lett.* **2008**, *93*, 052913.

(13) Arora, A. K.; Tandon, R. P.; Mansingh, A. Piezoelectric, Pyroelectric and Dielectric Properties of Lanthanum Modified Lead ZirconateTitanateCeramics. *Ferroelectrics* **1992**, *132*, 9−25.

(14) Karthik, J.; Martin, L. W. Pyroelectric Properties of Polydomain Epitaxial Pb(Zr$_{1-x}$Ti$_x$)O$_3$Thin Films. *Phys. Rev. B: Condens. Matter Mater. Phys.* **2011**, *84*, 024102.

(15) Karthik, J.; Agar, J. C.; Damodaran, A. R.; Martin, L. W. Effect of 90° Domain Walls and Thermal Expansion Mismatch on the Pyroelectric Properties of Epitaxial PbZr$_{0.2}$Ti$_{0.8}$O$_3$Thin Films. *Phys. Rev. Lett.* **2012**, *109*, 257602.

(16) Karthik, J.; Damodaran, A. R.; Martin, L. W. Effect of 90° Domain Walls on the Low-Field Permittivity of PbZr$_{0.2}$Ti$_{0.8}$O$_3$Thin Films. *Phys. Rev. Lett.* **2012**, *108*, 167601.

(17) Tang, Y.; Zhang, S.; Shen, Z.; Jiang, W.; Luo, J.; Sahul, R.; Shrout, T. R. Primary and Secondary Pyroelectric Coefficients of Rhombohedral and Tetragonal Single-Domain Relaxor-PbTiO$_3$Single Crystals. *J. Appl. Phys.* **2013**, *114*, 084105.

(18) Zook, J. D.; Liu, S. T. Pyroelectric Effects in Thin Film. *J. Appl. Phys.* **1978**, *49*, 4604−4606.

(19) Kosorotov, V. F.; Kremenchugskij, L. S.; Levash, L. V.; Shchedrina, L. V. Tertiary Pyroelectric Effect in Lithium Niobate and Lithium TantalateCrystals. *Ferroelectrics* **1986**, *70*, 27−37.

(20) Karthik, J.; Martin, L. W. Effect of Domain Walls on the Electrocaloric Properties of Pb(Zr$_{1-x}$Ti$_x$)O$_3$ Thin Films. *Appl. Phys. Lett.* **2011**, *99*, 032904.

(21) Li, X.; Lu, S.-G.; Chen, X.-Z.; Gu, H.; Qian, X.-S.; Zhang, Q. M. Pyroelectric and Electrocaloric Materials. *J. Mater. Chem. C* **2013**, *1*, 23−37.

(22) Pandya, S. P.; Wilbur, J. D.; Bhatia, B.; Damodaran, A. R.; Monachon, C.; Dasgupta, A.; King, W. P.; Dames, C.; Martin, L. W.

Direct Measurement of Pyroelectric and Electrocaloric Effects in Thin Films. *Phys. Rev. Appl.* **2017**, *7*, 034025.
(23) Hanrahan, B.; Espinal, Y.; Nevile, C.; Rudy, R.; Rivas, M.; Smith, A.; Kesim, M. T.; Aplay, S. P. Accounting for the Various Contributions to Pyroelectricity in Lead ZirconateTitanate Thin Films. *J. Appl. Phys.* **2018**, *123*, 124104.
(24) Pandya, S.; Damodaran, A. R.; Xu, R.; Hsu, S. L.; Agar, J. C.; Martin, L. W. Strain-Induced Growth Instability and Nanoscale Surface Patterning in Perovskite Thin Films. *Sci. Rep.* **2016**, *6*, 26075.
(25) Pandya, S.; Velarde, G. A.; Gao, R.; Everhardt, A. S.; Wilbur, J. D.; Xu, R.; Maher, J. T.; Agar, J. C.; Dames, C.; Martin, L. W. Understanding the Role of Ferroelastic Domains on the Pyroelectric and Electrocaloric Effects in Ferroelectric Thin Films. *Adv. Mater.* **2019**, *31*, 1803312.
(26) Damodaran, A. R.; Agar, J. C.; Pandya, S.; Chen, Z.; Dedon, L.; Xu, R.; Apgar, B.; Saremi, S.; Martin, L. W. New Modalities of Strain-Control of Ferroelectric Thin Films. *J. Phys.: Condens. Matter* **2016**, *28*, 263001.
(27) Dames, C. *Annual Review of Heat Transfer*; Begell House: New York, 2013; Vol. *16*, pp 7−48.
(28) Tong, T.; Karthik, J.; Martin, L. W.; Cahill, D. G. Secondary Effects in Wide Frequency Range Measurements of the Pyroelectric Coefficient of $Ba_{0.6}Sr_{0.4}TiO_3$ and $PbZr_{1-x}Ti_xO_3$Epitaxial Layers. *Phys. Rev. B: Condens. Matter Mater. Phys.* **2014**, *90*, 155423.
(29) Xu, F.; Trolier-McKinstry, S.; Ren, W.; Xu, B.; Xie, Z.-L.; Hemker, K. J. Domain Wall Motion and its Contribution to the Dielectric and Piezoelectric Properties of Lead ZirconateTitanate-Films. *J. Appl. Phys.* **2001**, *89*, 1336−1348.
(30) Agar, J. C.; Mangalam, R. V. K.; Damodaran, A. R.; Velarde, G.; Karthik, J.; Okatan, M. B.; Chen, Z. H.; Jesse, S.; Balke, N.; Kalinin, S. V.; Martin, L. W Tuning Susceptibility via Misfit Strain in Relaxed Morphotropic Phase Boundary $PbZr_{1-x}Ti_xO_3$ Epitaxial Thin Films. *Adv. Mater. Interfaces* **2014**, *1*, 140098.
(31) Ang, C.; Yu, Z. Dielectric Behavior of $PbZr_{0.52}Ti_{0.48}O_3$ Thin Films: Intrinsic and Extrinsic Dielectric Responses. *Appl. Phys. Lett.* **2004**, *85*, 3821−3823.
(32) Cahill, D. G. Thermal Conductivity Measurement from 30 to 750 K: the 3ω Method. *Rev. Sci. Instrum.* **1990**, *61*, 802−808.
(33) Pandya, S.; Wilbur, J.; Kim, J.; Gao, R.; Dasgupta, A.; Dames, C.; Martin, L. W. Pyroelectric Energy Conversion with Large Energy and Power Density in Relaxor Ferroelectric Thin Films. *Nat. Mater.* **2018**, *17*, 432−438.
(34) Ye, C.-P.; Tamagawa, T.; Polla, D. L. Experimental Studies on Primary and Secondary Pyroelectric Effects in $Pb(Zr_1$.xTix)O_3, $PbTiO_3$, and ZnOThin Films. *J. Appl. Phys.* **1991**, *70*, 5538−5543.
(35) Lang, S. Pyroelectric Coefficient of Lithium Sulfate Monohydrate (4.2−320 K). *Phys. Rev. B* **1971**, *4*, 3603−3609.
(36) Kurz, N.; Lu, Y.; Kirste, L.; Reusch, M.; Zukauskaite, A.; Lebedev, V.; Ambacher, O. Temperature Dependence of the Pyroelectric Coefficient of AlScNThin Films. *Phys. Status Solidi A* **2018**, *215*, 1700831.
(37) Damjanovic, D. Ferroelectric, Dielectric and Piezoelectric Properties of Ferroelectric Thin Films and Ceramics. *Rep. Prog. Phys.* **1998**, *61*, 1267−1324.
(38) Haun, M. J.; Furman, E.; Jang, S. J.; Cross, L. E. Thermodynamic Theory of the Lead Zirconate-TitanateSolid Solution System, Part V: Theoretical Calculations. *Ferroelectrics* **1989**, *99*, 63−86.
(39) Damodaran, A. R.; Pandya, S.; Agar, J. C.; Cao, Y.; Vasudevan, R. K.; Xu, R.; Saremi, S.; Li, Q.; Kim, J.; McCarter, M. R.; Dedon, L. R.; Angsten, T.; Balke, N.; Jesse, S.; Asta, M.; Kalinin, S. V.; Martin, L. W. Three-State Ferroelastic Switching and Large Electromechanical Responses in $PbTiO_3$ ThinFilms. *Adv. Mater.* **2017**, *29*, 1702069.
(40) Pertsev, N. A.; Zembilgotov, A. G.; Tagantsev, A. K. Effect of Mechanical Boundary Conditions on Phase Diagrams of Epitaxial Ferroelectric Thin Films. *Phys. Rev. Lett.* **1998**, *80*, 1988−1991.
(41) Noheda, B.; Gonzalo, J. A.; Cross, L. E.; Guo, R.; Park, S.-E.; Cox, D. E.; Shirane, G. Tetragonal-to-Monoclinic Phase Transition in a Ferroelectric Perovskite: theStructure of $PbZr_{0.52}Ti_{0.48}O_3$. *Phys. Rev. B: Condens. Matter Mater. Phys.* **2000**, *61*, 8687−8695.
(42) Noheda, B.; Cox, D. E.; Shirane, G. A Monoclinic Ferroelectric Phase in the $Pb(Zr_1$.xTix)O_3Solid Solution. *Appl. Phys. Lett.* **1999**, *74*, 2059−2061.
(43) Noheda, B.; Cox, D. E.; Shirane, G.; Guo, R.; Jones, B.; Cross, L. E. Stability of the Monoclinic Phase in the Ferroelectric Perovskite $PbZr_{1-x}Ti_xO_3$. *Phys. Rev. B: Condens. Matter Mater. Phys.* **2000**, *63*, 014103.
(44) Chynoweth, A. G. Dynamic Method for Measuring the Pyroelectric Effect with Special Reference to Barium Titanate. *J. Appl. Phys.* **1956**, *27*, 78−84.
(45) Byer, R. L.; Roundy, C. B. Pyroelectric Coefficient Direct Measurement Technique and Application to a NsecResponse Time Detector. *IEEE Trans. Sonics Ultrason.* **1972**, *3*, 333−338.
(46) Garn, L. E.; Sharp, E. J. Use of Low-Frequency Sinusoidal Temperature Waves to Separate Pyroelectric Currents from Non-pyroelectricCurrents. Part I. Theory. *J. Appl. Phys.* **1982**, *53*, 8974−8979.